

Interpretable Image Clustering via Diffeomorphism-Aware K -Means

Romain Cosentino
Rice University

Randall Balestriero
Rice University

Yanis Bahroun
Flatiron Institute

Anirvan Sengupta
Flatiron Institute & Rutgers University

Richard Baraniuk
Rice University

Behnaam Aazhang
Rice University

Abstract

We design an interpretable clustering algorithm aware of the nonlinear structure of image manifolds. Our approach leverages the interpretability of K -means applied in the image space while addressing its clustering performance issues. Specifically, we develop a measure of similarity between images and centroids that encompasses a general class of deformations: diffeomorphisms, rendering the clustering invariant to them. Our work leverages the Thin-Plate Spline interpolation technique to efficiently learn diffeomorphisms best characterizing the image manifolds. Extensive numerical simulations show that our approach competes with state-of-the-art methods on various datasets.

1. Introduction

With the amount of observations increasing in every field, from biological experiments to digital advertisement, it has become essential to develop machine learning algorithms capable of analyzing subtle structures present in data. Despite recent giant strides in supervised learning, the cost and need for an expert to provide the supervision remain substantial limitations. Thus, unsupervised learning algorithms, which are less dependent on expert knowledge, remain crucial for discovering patterns in big data [1, 2]. A specific branch of unsupervised learning central to our work is *clustering*. Clustering algorithms aim to organize data into groups based on distinct similarities and are often considered a bridge between supervised and unsupervised learning. It is important that clustering be interpretable both for data exploration and for deriving insights [3, 4].

The K -means clustering algorithm [5] is well-known for its simplicity, efficiency, and, in particular, interpretability. An integral part of the design of such a clustering algorithms is the choice of an appropriate metric space [6–8]. The clustering of data points requires measuring the distance between each of them and the centroids for the correct assignment to

a cluster. The commonly used K -means algorithm relies on the Euclidean distance. However, when dealing with metric spaces, one often has to choose between computational efficiency and the explanatory power of the relationship that is extracted. While the Euclidean distance makes the design of efficient algorithms easy, this measure of similarity might miss subtle relationships between data points that are not superficially close by. Defining an appropriate measure of similarity between images lying in high-dimensional spaces is a critical bottleneck to high-performance clustering algorithms [9].

A recent way to extract nonlinear relationships between data is built upon the concept of invariance [10–14]. In this work, we are particularly interested in measures of similarity that incorporate the action of a transformation on the data into its very definition. In computer vision, the study of affine invariant distance has a long tradition, initially inspired by neuroscience observations. In the early 1940s, the pioneering work in [15] suggested that the multi-layer network underlying our vision acts as a similarity detector that enables the detection of classes of equivalences and is still being actively investigated [16, 17].

These findings have later been leveraged to provide powerful unsupervised computer vision algorithms [18–20]. When applied to images, these pioneering techniques usually require each image to be landmarked, i.e., to have annotated points on their most essential features [21]. Another critical set of work, e.g, the works in [11, 22–25], focused on visual appearance instead of shape. They proposed the development of features that are invariant to specific transformations. However, it was noted that extracting these features reliably and consistently is not easy [26]. In the same vein, the use of the Dynamic Time Warping algorithm on flattened images has been used to understand and compare images being the results of transformations [27–29].

The approach that has most inspired our work considers images as points in a high-dimensional space. In this space,

similarities in appearance between images are quantified by their geometric proximity [30]. These methods are referred to as appearance manifold-based approaches and have been successfully used to cluster images [31–33]. Notable work [26, 34, 35] has introduced several distances, which followed the development of metrics capturing symmetries in the data. A key observation of the authors was that the Euclidean distance between two images of faces of different individuals but with the same pose is always smaller than the Euclidean distance between two images of the same individual’s faces in different poses. From these observations, in [26, 34, 35], the authors clearly expressed the need for distances to distinguish data based on their taxonomy and be invariant to their orientations, position in the images, and illumination conditions. Whereas the approaches mentioned above appear general, they are limited to the affine case, when in practice, images like in the example aforementioned are subject to more intricate and non-rigid symmetries.

In this work, we show that it is essential to consider a broader class of transformations, diffeomorphisms, to capture the complex transformations an image can undertake while preserving its original identity. We thus develop a similarity measure that is invariant to this general class of deformation. As a result, by combining the popular K -means with our measure, we introduce the Deformation Invariant K -means (DI K -means) algorithm. Our approach is displaying improved performance on benchmarks, outperforming the Affine Invariant K -means as well as competing with state-of-the-art models.

Our contributions can be summarized as follows:

- We define an efficient parametrization of image transformations with respect to diffeomorphisms, Sec. 2.
- We introduce the *Deformation Invariant K-means algorithm* that addresses the limitations of the Affine Invariant K -means approach, as well as a novel centroid update rule that enables the learnability of centroid lying on the image manifold, Sec. 3.
- Finally, we show numerically that our unsupervised algorithm competes with state-of-the-art methods on various datasets while benefiting from interpretable results, Sec. 4.

2. Image Transformations

In this work, we build a measure that enables us to capture the symmetries in the data. To do so, we focus our interest on the action of groups of transformation on the data. By action of a group on an image, we refer to the deformation of this image with respect to a particular transformation induced by a group. For instance, the rotation, translation, and shearing of an image can be considered the result of the action of elements of the affine group. An introduction to group transformations can be found in [36].

In this section, we present two popular groups of transformation in computer vision, the affine and the diffeomorphism group, denoted by $\text{Aff}(\mathbb{R}^2)$ and $\text{Diff}(\mathbb{R}^2)$, respectively.

2.1. Transformation Groups

The groups of transformation that we consider is applied to the coordinates of the pixels of an image, characterized by the real plane, \mathbb{R}^2 . For example, in Fig. 1, the image is characterized by the intensity of the pixels located on a grid of \mathbb{R}^2 . A transformation then acts on an image by changing the coordinates of its pixels in the plane, as shown by the deformed grids in Fig. 1. Then given a transformation of the pixel coordinates, represented by a grid, the transformed image is rendered by bilinear interpolation as in Fig. 1.

Unlike previous work, we not only exploit the affine group, $\text{Aff}(\mathbb{R}^2)$, consisting of only 6 parameters, but also the group of diffeomorphisms, $\text{Diff}(\mathbb{R}^2)$. The elements of $\text{Diff}(\mathbb{R}^2)$ are smooth and possibly nonlinear functions acting on \mathbb{R}^2 , again representing the coordinates of the pixels of an image. In Fig. 1, we show an example of a diffeomorphic transformation applied to the digit 4. It is important to note that the linearity of a transformation of pixel coordinates of a given image does not imply a linear transformation of the given image. For instance, the translation of an image is a linear operator in the coordinate space but highly nonlinear in the high-dimensional image space [37].

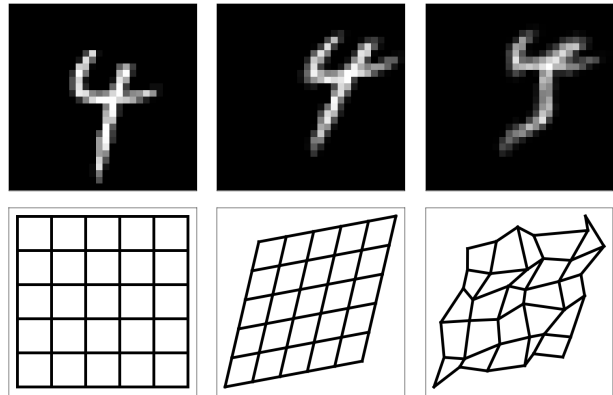


Figure 1: **Image Transformations** - Visualizations of a sample taken from the MNIST dataset and its transformed versions. Each image results from the application of the transformation induced by the grid displayed below it. (Left) we observe the original image and its associated original transformation grid, which corresponds to the identity transform. (Middle) the image has been transformed by the affine transformation induced by the associated grid. (Right) the image transformed by the diffeomorphism using the TPS induced by the grid below it. Note that the associated grid on the bottom right is a diffeomorphism generalizing affine transformations.

2.2. A Parametric Approach to Diffeomorphisms

We consider as diffeomorphism a (smooth) mapping from \mathbb{R}^2 to \mathbb{R}^2 that transforms the coordinates of an input (image) to produce a deformed one [38]. We choose to parametrize such a mapping by using a polyharmonic spline, specified by finitely many parameters. In particular, we consider the Thin-Plate-Spline (TPS) interpolation technique [39], which is also one of the most widely used transformations approximation methods in image registration problems dealing with nonlinear geometric differences [40, 41]. Essential to our work, the TPS is the biharmonic radial basis function that produces smooth surfaces from \mathbb{R}^2 to \mathbb{R}^2 , which are infinitely differentiable [42]. In particular, it provides a transformation map that minimizes the volume described by the sum of the squares of the second derivative terms of the interpolant function, also referred to as the Biharmonic equations without boundary conditions [43]. In particular, We refer the reader to App. 10 for details regarding this method.

In this work, we consider as learnable parameters of the TPS a set of 2-dimensional coordinates, called landmarks, and denoted by ν . Given a set of landmarks, the TPS provides the parameters of the radial basis function performing the transformation map. That is, the euclidean plane is bent according to the learned landmarks. While we optimize the landmarks directly, an alternative approach proposed in [44, 45] predicted them using a deep neural network. In Fig. 1, we can see on the bottom right, the grid associated with the $\ell = 6^2$ landmarks that enable the diffeomorphic transformation of the 4.

The TPS transformation of an image $x \in \mathbb{R}^n$, with ℓ -landmarks, is written as

$$\text{TPS}_\ell(x; \nu) , \quad (1)$$

with $\nu \in \mathbb{R}^{2\ell}$, that is, ℓ , 2-dimensional coordinates.

3. Deformation Invariant K -means

We now introduce our main contribution: the DI K -means algorithm. The DI K -means combines the K -means' centroids-based clustering approach with a measure of similarity that we design to be invariant to diffeomorphisms.

3.1. Diffeomorphism-aware Similarity Measure

Given a set of images $\{x_i\}_{i=1}^N$, with $x_i \in \mathbb{R}^n$, the K -means algorithm aims at grouping the data into K distinct clusters defining the partition $\mathcal{C} = \{C_k\}_{k=1}^K$, with $\cup_k C_k = \{x_i\}_{i=1}^N$ and $C_i \cap C_j = \emptyset, \forall i \neq j$. Each cluster C_k of the partition is represented by a centroid $\mu_k \in \mathbb{R}^n, \forall k \in \{1, \dots, K\}$.

The goal of the DI K -means is to find the centroids minimizing the following distortion error

$$\min_{\mathcal{C}, \mu_1, \dots, \mu_K, \forall k, \|\mu_k\|_2=1} \sum_{k=1}^K \sum_{i: x_i \in C_k} d(x_i, \mu_k) . \quad (2)$$

The assignment of an image x_i to a cluster C_k is achieved through the evaluation of the similarity measure, d , between the image and each centroid. An image x_i belongs to cluster C_l if and only if $l = \arg \min_k d(x_i, \mu_k)$. While the standard K -means algorithm makes use of the Euclidean distance, i.e., $d(x_i, \mu_k) = \|x_i - \mu_k\|_2^2$, we instead propose to use the following deformation invariant similarity measure

$$d(x_i, \mu_k) := \min_{\nu \in \mathbb{R}^{2\ell}} \|\text{TPS}_\ell(x_i; \nu) - \mu_k\|_2^2 . \quad (3)$$

This similarity measure characterizes the fitting of the TPS transformation of the image x_i to best fit the centroid μ_k in the least-square sense. Note that it is a *Quasipseudosemi-metric*, see App. 7 for details and proof. This measure requires solving a non-convex optimization problem. It can be achieved in practice by exploiting the differentiability of the TPS with respect to the landmarks ν . As a result, we can learn the transformation by performing gradient-descent based optimization [46]; further details regarding this optimization are given in Appendix 8 as well as solutions to facilitate optimization of the non-convex objective by exploiting the image manifold geometry.

The essential property of the measure we propose is its invariance to deformations, formal proofs and definitions in Appendix 7.3.

3.2. Learning the DI K -means

Solving the optimization problem in Eq. 2, similarly to K -means, is an NP-hard problem. A popular tractable solution nonetheless exists and is known as the two-step Lloyd algorithm [47].

In the DI K -means, the first step of the Lloyd algorithm consists of assigning the images to a cluster using the newly defined measure of similarity in Eq. 3. The second step, is the update of the centroids using the previously determined cluster assignment. It corresponds to the result of the optimization problem: $\arg \min_{\mu_k: \|\mu_k\|=1} \sum_{i: x_i \in C_k} d(x_i, \mu_k)$, which solution is the following Proposition 1.

Proposition 1. *The centroids update of the DI K -means algorithm are given by*

$$\mu_k^* \propto \frac{1}{|C_k|} \sum_{i: x_i \in C_k} \text{TPS}_\ell(x_i; \nu_{i,k}^*), \quad \forall k \quad (4)$$

where $|C_k|$ denotes the cardinal of the set C_k , $\nu_{i,k}^*$ is the set of parameters of the TPS that best transforms the image x_i to the centroid μ_k defined in Eq. 3, and \propto defines the proportionality relation (proof in App. 7.2).

The averaging in Eq. 4 is performed on the transformed version of the images. DI K -means thus considers the topology of the images' ambient space. A pseudo-code of the centroid update Eq. 4 is presented in Algo. 1.

The training of the DI K -means, which aims at minimizing the distortion error Eq. 2 is done by alternating between

Algorithm 1 Centroids Updates of DI K -means

Input: Cluster C_k , TPS parameters $\{\nu_{i,k}^*\}_{i:x_i \in C_k}$

Output: Centroids update μ_k^*

- 1: Initialize $\mu_k = 0$
 - 2: **for** $i : x_i \in C_k$ **do**
 - 3: Compute $\mu_k = \mu_k + \text{TPS}_\ell(x_i; \nu_{i,k}^*)$, Eq. 4
 - 4: $\mu_k^* = \frac{\mu_k}{|C_k|}$
-

the two steps detailed above, until a stopping criterion is met, and is summarized in Algo. 2.

Algorithm 2 Deformation Invariant K -means

Input: Initial centroids μ_k , dataset $\{x_i\}_{i=1}^N$

Output: Cluster partition $\{C_k\}_{k=1}^K$

- 1: **repeat**
 - 2: **for** $i = 1$ to N **do**
 - 3: **for** $k = 1$ to K **do**
 - 4: Compute and store $d(x_i, \mu_k)$ by solving Eq. 3
 - 5: Assign x_i to C_l where $l = \arg \min_k d(x_i, \mu_k)$
 - 6: Update the centroid μ_k using Algo. 1
 - 7: **until** Stopping criterion
-

The update Eq. 4 induced by our similarity measure alleviates a fundamental limitation of the standard K -means when applied in the pixel space of the images. In fact, in the standard K -means, the average of the data belonging to a cluster C_k , $\frac{1}{|C_k|} \sum_{i:x_i \in C_k} x_i$, consists of an averaging in the pixel space, which as a result does not account for the non-Euclidean geometry of the image manifold [48, 49]. For example, when considering faces, the naive “average face” of an individual over different poses based on the Euclidean distance does not correspond to a recognizable picture of that individual.

3.3. Computational Complexity & Parameters

The time complexity of DI K -means is $O(NK(\ell^3 + \ell n))$. In fact, the DI K -means computes a TPS of computational complexity $O(\ell^3 + \ell n)$ for each sample of the N samples and each of the K centroids, as in Eq. 3. The number of parameters of the model is $2\ell \times N \times K$, it depends on the number of samples, clusters, and landmarks.

To speed up the computation, we 1) pre-compute the matrix inverse responsible for the dominating cubic term, see Appendix 10 for implementation details regarding the TPS, and 2) implement DI K -means on GPU with SymJAX [50] where high parallelization renders the practical computation time near constant with respect to the number of landmarks as we depict in Fig. 2.

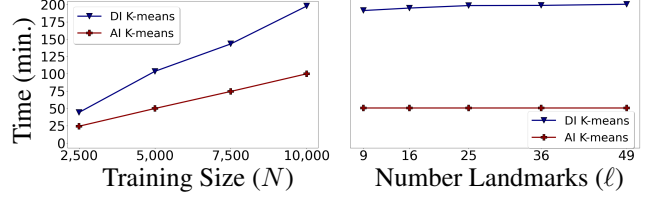


Figure 2: **Computational Training Time** - Comparison between our DI K -means and the AI K -means computational times on the Arabic Characters dataset. The input pixel size is $n = 1024$. (Left) shows the computational time for varying training set size and $\ell = 7^2$. (Right) shows the variations as a function of the number of landmarks, ℓ , for $N = 10,000$. Since the AI K -means does not use the TPS algorithm, its computational time is constant as a function of the number of landmarks.

4. Experimental Setup and Cross Validation

In this section, we detail the experimental setting followed to evaluate the performance of our model as well as important details on the cross-validation of the various models. It is important to note that our model operates in the unsupervised settings, thus we do not compare our method with models trained leveraging the cluster membership labels. Also, for all clustering algorithms, the number of clusters is set to be the number of classes the dataset contains. The various datasets used are described in Appendix 11.

4.1. Evaluation Metric

For all the experiments, the accuracy is calculated using the metric proposed in [51] and defined as

$$\text{Accuracy} = \max_m \frac{1}{N} \sum_{i=1}^N 1_{\{l_i = m(\hat{l}_i)\}}, \quad (5)$$

where l_i is the ground-truth label, \hat{l}_i the cluster assignment and m all the possible one-to-one mappings between clusters and labels. The results in Table 1 are taken as the best score on the test set based on the ground truth labels among 10 runs as in [52].

4.2. Competing Models

We compare our model with well-known clustering techniques using deep neural networks. We performed experiments for the VaDE [53] and DEC [52] using the code made publicly available by the authors. We use the annotation (MLP) as a reference to the MLP architecture used in their experiments (see App. 9 for details). To fairly compare our model to the DEC and VaDE models, we proposed a convolutional architecture to the DEC and VaDE networks, denoted by DEC (Conv) and VaDE (Conv) (see App. 9 for details). Finally, we evaluate the performance of an augmented K -means algorithm trained using the features extracted by an

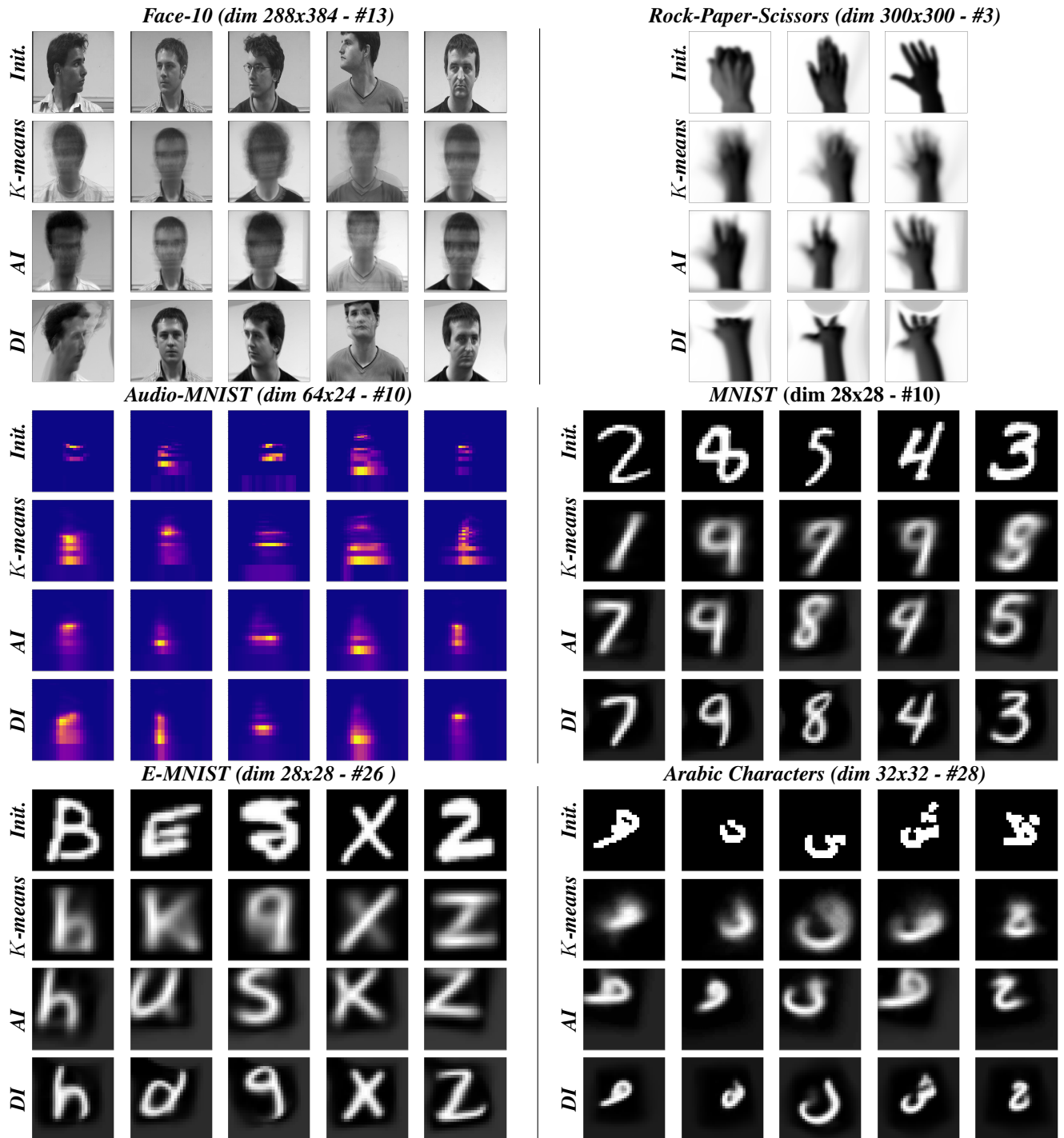


Figure 3: **Centroids** - The name of the datasets considered is written on top of each subfigure, and # corresponds to the number of classes. For each dataset, we depict the centroids at initialization in the top row. The centroids learned by K -means are shown in the 2nd row, by the Affine invariant K -means in the 3rd row, and by our DI K -means in the 4th row. By comparing the results of the AI K -means (3rd row) with the standard K -means (2nd row), we can see that using only affine transformations slightly improves the K -means centroids and reduces the superposition issue that K -means suffers from. By comparing the results of our DI K -means (4th row) with the other methods, it is clear that using the more general class of transformation that are diffeomorphisms, via the TPS, significantly improves the centroids, making them sharper and removing the issue related to the non-additiveness of images. Note that K -means iteratively updates the centroids and cluster assignments, as such, the class associated to a specific centroid usually changes during training .

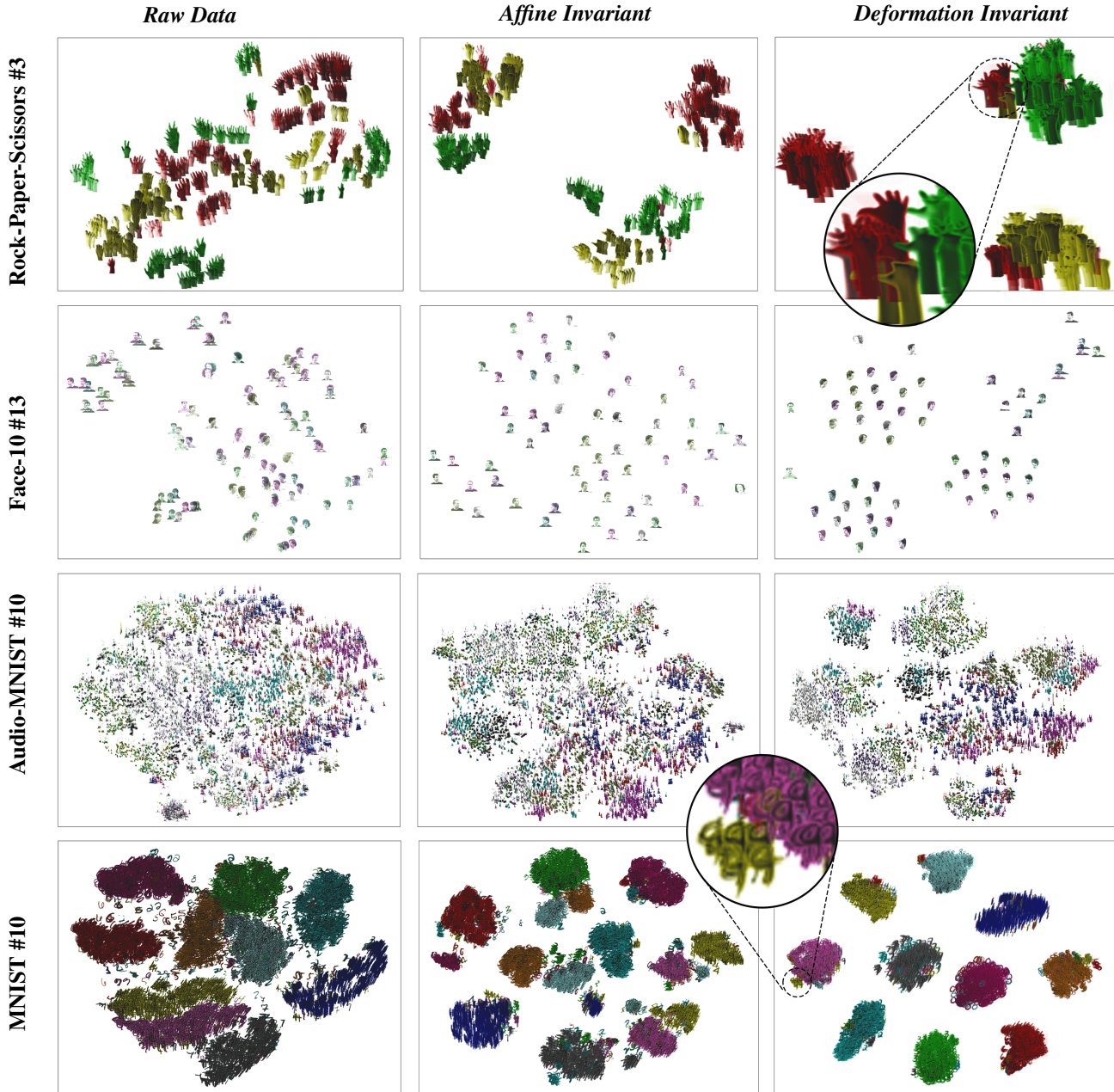


Figure 4: **2-dimensional t-SNE** - (# denotes the number of clusters) - We suggest the reader to zoom in the plots to best appreciate the visualization. - The raw data (*left column*), the affinely transformed data using the AI distance, i.e., we extract the best affine transformation of the data that corresponds to the centroid it was assigned and perform the t-SNE on these affinely transformed data, (*middle column*), the data transformed with respect to the TPS as per Eq. 3, i.e., the same process as previously mentioned but we consider the transformation induced by the TPS, and then perform the dimension reduction on these transformed data, (*right column*). Each row corresponds to a different datasets, Rock-Paper-Scissor, Face-10, AudioMNIST, and MNIST are depicted from the top to bottom row. For all the figures, the colors of the data represent their ground truth labels. We observe that across datasets, both the affine transformation learned on the data and the TPS transformation help to define more localized clusters. One can observe that for the Face-10 dataset, while the dataset contains 13 clusters, we can see that the DI K -means induced transformations lead to a 2-dimensional space where the faces are clustered 3 majors orientations. The top left cluster corresponds to faces pointing left, the bottom one face pointing right, and the bottom right one face pointing front.

Autoencoder, denoted by AE + K -means in the following.

The parameters of the different models mentioned above are learned by stochastic gradient descent (Adam optimizer [46]). In all the experiments, the learning rate are cross-validated according to $[10^{-4}, 5 \times 10^{-4}, 10^{-3}, 5 \times 10^{-3}, 10^{-2}, 5 \times 10^{-2}]$. The internal parameters that are model dependant, e.g., the number of pre-training epoch and the update intervals, are also cross-validated.

We also compare our DI K -means to the closely related K -means and affine invariant K -means, denoted by AI K -means in the following. The AI K -means was designed to include only affine transformations. For each run, all three K -means algorithms start from the same initial centroids using the K -means++ algorithm developed by [54] to speed up the convergence of the K -means algorithm.

4.3. Cross Validation Settings

Our model requires the cross-validation of hyper-parameters related to the learnability of the transformation within the similarity measure, Eq. 3. However, the clustering framework does not allow the use of label information to perform the cross-validation of the parameters. We thus need to find a proxy for it to determine the optimal model parameters. Interestingly, the distortion error related used in the DI K -means, Eq. 2, appears to be negatively correlated to the accuracy, as displayed in Fig. 5. The use of the distortion error is commonly used as a fitness measure in K -means for example when cross-validating the number of clusters.

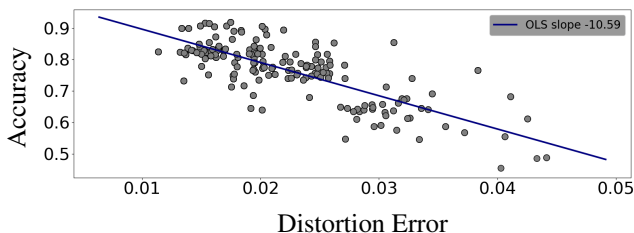


Figure 5: **Accuracy vs Distortion Error** - Clustering accuracy, Eq. 5, of DI K -means algorithm on the MNIST dataset as a function of the distortion error, Eq. 2, using the similarity measure, Eq. 3. Each gray dot is associated with a specific set of hyper-parameters, e.g., learning rate, number of landmarks for the TPS. The accuracy is negatively correlated to the distortion error (see the blue line corresponding to the ordinary least square fit), indicating that the distortion error is an appropriate metric to cross-validate the hyper-parameters of the DI K -means algorithm.

We cross-validate the number of landmarks, ℓ , which defines the resolution of the transformation, which we optimize over the following grid, $[3^2, 4^2, 5^2, 6^2, 7^2, 8^2]$. Then, the learning of the landmarks, ν , is done via Adam optimizer. The learning rate is picked according

to $[10^{-4}, 5 \times 10^{-4}, 10^{-3}, 5 \times 10^{-3}, 10^{-2}, 5 \times 10^{-2}]$. We train our method for 150 epochs for all the datasets, with batches of size 64. As for K -means and AI K -means, the centroids’ initialization of the DI K -means is performed by the K -means++ algorithm. Importantly, the same procedure is applied to all datasets.

Note that during the training, both the similarity measure in Eq. 3 and the clustering update are performed, Eq. 5. During the algorithm’s testing phase, the centroids remain fixed, and only the similarity measure is trained to assign each testing datum to a cluster. For a given testing sample, we find its best fit with respect to all centroids μ_k^* , $\forall k$, and assign it to the closest according to the DI similarity measure, Eq. 3.

5. Results and Interpretation

In this section, we report and interpret the results obtained by our DI K -means and competing models.

5.1. Clustering Accuracy

We report in Table 1 the accuracy of the various models considered on the different datasets. Our approach shows to outperform existing models on most datasets. Our model equals the performance of AI K -means on Affine MNIST and is only outperformed by VaDE (MLP) on MNIST. Whereas the various deep learning approaches perform well on datasets for which their architectures were developed, e.g., MNIST and its derivatives: E-MNIST, Arabic Characters, they show limited performance on higher resolution datasets with a small number of samples, such as Rock-Paper-Scissors, Face-10 as well as the two toy examples (composed of only 700 training data and 300 testing data).

5.2. Interpretability: Centroids Visualization

We propose in Fig. 3 to visualize the centroids obtained via K -means, AI K -means, and our DI K -means. Supplementary visualisations are provided in Appendix 12.2. For each dataset, the first row shows the clusters after initialization from K -means++, as mentioned in Sec. 4.2. The three following rows show the centroids obtained via the K -means, AI K -means, and DI K -means algorithms, respectively.

We observe that, for all datasets, the K -means centroids are not possible samples from the data. In that sense, the K -means algorithm does not consider the non-linear manifold structure of the data. In fact, its update rule consists in the average of the data belonging to each cluster in the pixel space, thus producing blurred and mixed centroids. The AI K -means algorithm drastically reduces the blurriness of the centroids induced by such an averaging as it considers the average of affinely transformed data. However, our DI K -means produces the crispest centroids and does not introduce any ambiguity in between the different clusters. In fact, the

Table 1: Clustering Results in % of the test set accuracy Eq. 5 - the number of clusters is denoted by # next to the dataset name.

<i>Models</i>	<i>Deep Learning</i>	<i>Affine MNIST #10</i>	<i>Diffeo. MNIST #10</i>	<i>MNIST #10</i>	<i>Audio MNIST #10</i>	<i>E-MNIST #26</i>	<i>Rock-Paper-Scissors #3</i>	<i>Face-10 #13</i>	<i>Arabic Char. #28</i>
<i>K</i> -means ([52])	✗	68.0	61.8	53.5	10.8	39.5	40.6	20.5	19.4
AI <i>K</i> -means	✗	100.0	91.7	75.3	29.8	48.0	72.8	31.2	30.25
DI <i>K</i> -means (Our)	✗	100.0	99.2	92.5	41.6	65.3	86.6	45.3	51.1
AE + <i>K</i> -means	✓	72.6	60.5	66.3	13.8	41.8	48.1	37.7	23.5
DEC (MLP) ([52])	✓	84.3	77.6	84.3	10.9	55.4	46.2	33.6	24.2
DEC (Conv)	✓	70.4	68.2	78.8	15.3	60.1	54.1	38.3	29.1
VaDE (MLP) ([53])	✓	68.8	65.4	94.1	11.3	20.3	50.3	36.4	26.2
VaDE (Conv)	✓	65.4	59.3	81.7	14.3	58.3	55.4	40.9	46.4

update of our method, Eq. 4, takes into account the non-linear structure of the image manifold by taking the average over diffeomorphically transformed data.

Interestingly, Fig. 3 shows that even if at initialization multiple centroids assigned to the same class are attributed to different clusters, the DI *K*-means is able to recover this poor initialization thanks to its explicit manifold modeling and centroid averaging technique. For instance, in the Rock-Paper-Scissors dataset, although at initialization, two centroids correspond to the class paper, the DI *K*-means learns centroids of each of the three classes within this dataset. In the Face-10 dataset, some centroids learned correspond to the rotation of the initialization, even in such extreme change of pose, the centroids remain crisp in most cases.

5.3. Interpretability: Embedding Visualization

To get further insights into the diffeomorphism-awareness and disentangling capability of the DI *K*-means, we compare the 2-dimensional projections of the data using t-SNE [55], of the *K*-means, AI *K*-means and DI *K*-means. Supplementary visualisations are provided in Appendix 12.1. The t-SNE visualizations, for both the AI and DI *K*-means, are obtained by extracting the optimal transformation that led to the assignment. Then t-SNE is then applied to all the transformed data using the optimal transformation.

We can observe in Fig. 4 that across datasets, the affine transformations help separate the data in this 2-dimensional space. The diffeomorphism-awareness of the DI *K*-means also drastically enhance the separability of the different clusters. When using DI *K*-means, the data are clustered based on macroscopically meaningful and interpretable parameters, making the model’s performance possible to understand. For instance, for the Face-10 dataset, the t-SNE representation of the DI *K*-means clusters’ shows that faces are grouped according to three significant orientations, left, right, and front. These three clusters are more easily observed in our DI *K*-means than in the affine invariant model. However, the 13 different orientations present in the dataset remain too subtle to be captured by the DI *K*-means. These observa-

tions could explain the improved clustering performance of our model.

For the MNIST dataset, the last row and column of Fig. 4, we observe that most of the incorrectly “classified” images are almost indistinguishable from samples of the other class. In particular, we highlight this by proposing to zoom-in into the cluster of 9 in Fig. 4. We can see that the yellow instances are samples from the class 4 that have been transformed such that they resemble the 9’s centroid in Fig. 3. Besides, the centroid of the cluster 4, in Fig. 3, has its upper part disconnected, while these transformed samples do not. We also provide a zoom-in on one of the clusters obtained on the rock-paper-scissors dataset, first row and last column of Fig. 4. The incorrectly clustered data are the ones that, when transformed, easily fit the scissor shape. In fact, we can see that both the transformed rock sample (yellow) and the paper (red) ones have the thumb pointing outward as the scissors centroid in Fig. 3.

The diffeomorphism-aware algorithm we propose is based on the transformation of any data into any centroid. Therefore, it depends on the number of landmarks, ℓ , which can create transformations that are too large for some data and not enough for others. While such a trade-off is sample dependant, the overall results display a large improvement compared to the two other interpretable methods.

6. Conclusion

We proposed a novel formulation of *K*-means suited to tackle clustering in computer vision tasks where image deformations should not affect the clustering of the algorithm. We did so by parametrizing this space of deformation with the TPS interpolation technique between images and centroids. Our technique reaches state-of-the-art performances while preserving the interpretability of the clustering as the centroids, and the TPS-transformed input images all live in the original data space. Interpretability of the model allows to easily diagnose failure cases, clustering decisions and should be favored in computer vision clustering application where explainability of the decision plays a role.

Acknowledgment

This work was supported by NSF grants SCH-1838873, CCF-1911094, IIS-1838177, and IIS-1730574; NIH grant R01HL144683-CFDA; ONR grants N00014-18-12571 and N00014-17-1-2551; AFOSR grant FA9550-18-1-0478; DARPA grant G001534-7500; and a Vannevar Bush Faculty Fellowship, ONR grant N00014-18-1-2047.

References

- [1] S. Dolnicar, “Using cluster analysis for market segmentation—typical misconceptions, established methodological weaknesses and some recommendations for improvement,” *Australasian Journal of Market Research*, vol. 11, no. 2, pp. 5–12, 2003. **1**
- [2] R. Xu and D. C. Wunsch, “Clustering algorithms in biomedical research: a review,” *IEEE Reviews in Biomedical Engineering*, vol. 3, pp. 120–154, 2010. **1**
- [3] D. Bertsimas, A. Orfanoudaki, and H. Wiberg, “Interpretable clustering: an optimization approach,” *Machine Learning*, pp. 1–50, 2020. **1**
- [4] D. Greene and P. Cunningham, “Producing accurate interpretable clusters from high-dimensional data,” in *European Conference on Principles of Data Mining and Knowledge Discovery*, pp. 486–494, Springer, 2005. **1**
- [5] J. MacQueen, “Some methods for classification and analysis of multivariate observations,” in *Proceedings of the Fifth Berkeley Symposium on Mathematical Statistics and Probability, Volume 1: Statistics*, (Berkeley, Calif.), pp. 281–297, University of California Press, 1967. **1**
- [6] K. He, F. Wen, and J. Sun, “K-means hashing: An affinity-preserving quantization method for learning binary compact codes,” in *IEEE Conference on Computer Vision and Pattern Recognition*, pp. 2938–2945, 2013. **1**
- [7] B. J. Frey and N. Jojic, “Fast, large-scale transformation-invariant clustering,” in *Advances in Neural Information Processing Systems*, pp. 721–727, 2002. **1**
- [8] B. Raytchev and H. Murase, “Unsupervised face recognition from image sequences based on clustering with attraction and repulsion,” in *IEEE Computer Society Conference on Computer Vision and Pattern Recognition.*, vol. 2, pp. II–II, IEEE, 2001. **1**
- [9] M. Steinbach, L. Ertöz, and V. Kumar, “The challenges of clustering high dimensional data,” in *New Directions in Statistical Physics*, pp. 273–309, Springer, 2004. **1**
- [10] S. Mallat, “Understanding deep convolutional networks,” *Philosophical Transactions of the Royal Society A: Mathematical, Physical and Engineering Sciences*, vol. 374, no. 2065, p. 20150203, 2016. **1**
- [11] J. Bruna and S. Mallat, “Invariant scattering convolution networks,” *IEEE Transactions on Pattern Analysis and Machine Intelligence*, vol. 35, no. 8, pp. 1872–1886, 2013. **1**
- [12] E. Oyallon, E. Belilovsky, and S. Zagoruyko, “Scaling the scattering transform: Deep hybrid networks,” in *IEEE International Conference on Computer Vision*, pp. 5618–5627, 2017. **1**
- [13] T. Cohen, M. Weiler, B. Kicanaoglu, and M. Welling, “Gauge equivariant convolutional networks and the icosahedral cnn,” *arXiv preprint arXiv:1902.04615*, 2019. **1**
- [14] J. Andén and S. Mallat, “Deep scattering spectrum,” *IEEE Transactions on Signal Processing*, vol. 62, no. 16, pp. 4114–4128, 2014. **1**
- [15] W. Pitts and W. S. McCulloch, “How we know universals the perception of auditory and visual forms,” *The Bulletin of Mathematical Biophysics*, vol. 9, no. 3, pp. 127–147, 1947. **1**
- [16] N. Kriegeskorte, M. Mur, D. A. Ruff, R. Kiani, J. Bodurka, H. Esteky, K. Tanaka, and P. A. Bandettini, “Matching categorical object representations in inferior temporal cortex of man and monkey,” *Neuron*, vol. 60, no. 6, pp. 1126–1141, 2008. **1**
- [17] A. Sengupta, C. Pehlevan, M. Tepper, A. Genkin, and D. Chklovskii, “Manifold-tiling localized receptive fields are optimal in similarity-preserving neural networks,” in *Advances in Neural Information Processing Systems*, pp. 7080–7090, 2018. **1**
- [18] D. G. Kendall, D. Barden, T. K. Carne, and H. Le, *Shape and shape theory*, vol. 500. John Wiley & Sons, 2009. **1**
- [19] M. Werman and D. Weinshall, “Similarity and Affine Invariant Distances Between 2d Point Sets,” *IEEE Transactions on Pattern Analysis and Machine Intelligence*, vol. 17, no. 8, pp. 810–814, 1995. **1**
- [20] R. Berthilsson, “A statistical theory of shape,” in *Joint IAPR International Workshops on Statistical Techniques in Pattern Recognition (SPR) and Structural and Syntactic Pattern Recognition (SSPR)*, pp. 677–686, Springer, 1998. **1**
- [21] E. Begelfor and M. Werman, “Affine invariance revisited,” in *Computer Society Conference on Computer Vision and Pattern Recognition*, vol. 2, pp. 2087–2094, IEEE, 2006. **1**
- [22] L. Sifre and S. Mallat, “Rotation, scaling and deformation invariant scattering for texture discrimination,” in *IEEE Conference on Computer Vision and Pattern Recognition*, June 2013. **1**
- [23] W. Czaja, I. Kavalero, and W. Li, “Scattering transforms and classification of hyperspectral images,” in *Algorithms and Technologies for Multispectral, Hyperspectral, and Ultraspectral Imagery XXIV*, vol. 10644, p. 106440H, 2018. **1**
- [24] D. Charalampidis, “A modified k-means algorithm for circular invariant clustering,” *IEEE Transactions on Pattern Analysis and Machine Intelligence*, no. 12, pp. 1856–1865, 2005. **1**
- [25] B. Le Saux and N. Boujemaa, “Unsupervised robust clustering for image database categorization,” in *Object Recognition Supported by User Interaction for Service Robots*, vol. 1, pp. 259–262, IEEE, 2002. **1**

- [26] J. Lim, J. Ho, M.-H. Yang, K.-c. Lee, and D. Kriegman, "Image clustering with metric, local linear structure, and affine symmetry," in *European Conference On Computer Vision*, pp. 456–468, Springer, 2004. [1](#), [2](#), [13](#)
- [27] T. M. Rath and R. Manmatha, "Word image matching using dynamic time warping," in *IEEE Conference on Computer Vision and Pattern Recognition.*, vol. 2, pp. II–II, IEEE, 2003. [1](#)
- [28] A. L. Ratan, W. E. L. Grimson, and W. M. Wells, "Object detection and localization by dynamic template warping," *International Journal of Computer Vision*, vol. 36, no. 2, pp. 131–147, 2000. [1](#)
- [29] K. Santosh, "Use of dynamic time warping for object shape classification through signature," *Kathmandu University Journal of Science, Engineering and Technology*, vol. 6, no. 1, pp. 33–49, 2010. [1](#)
- [30] H. Murase and S. K. Nayar, "Learning and recognition of 3d objects from appearance," in *Proceedings IEEE Workshop on Qualitative Vision*, pp. 39–50, 1993. [2](#)
- [31] R. Basri, D. Roth, and D. Jacobs, "Clustering appearances of 3d objects," in *Computer Society Conference on Computer Vision and Pattern Recognition*, pp. 414–420, IEEE, 1998. [2](#)
- [32] M.-C. Su and C.-H. Chou, "A Modified Version of the K-means Algorithm with a Distance Based on Cluster Symmetry," *IEEE Transactions on Pattern Analysis and Machine Intelligence*, vol. 23, no. 6, pp. 674–680, 2001. [2](#)
- [33] J. Ho, M.-H. Yang, J. Lim, K.-C. Lee, and D. Kriegman, "Clustering appearances of objects under varying illumination conditions," in *IEEE Computer Society Conference on Computer Vision and Pattern Recognition.*, vol. 1, pp. I–I, IEEE, 2003. [2](#)
- [34] A. Fitzgibbon and A. Zisserman, "On affine invariant clustering and automatic cast listing in movies," in *European Conference on Computer Vision*, pp. 304–320, Springer, 2002. [2](#), [13](#)
- [35] P. Y. Simard, Y. A. LeCun, J. S. Denker, and B. Victorri, "Transformation invariance in pattern recognition—tangent distance and tangent propagation," in *Neural Networks: Tricks of the Trade*, pp. 235–269, Springer, 2012. [2](#), [13](#)
- [36] B. Hall, *Lie groups, Lie Algebras, and Representations: an Elementary Introduction*, vol. 222. Springer, 2015. [2](#)
- [37] R. P. Rao and D. L. Ruderman, "Learning lie groups for invariant visual perception," in *Advances in Neural Information Processing Systems*, pp. 810–816, 1999. [2](#)
- [38] L. Younes, *Shapes and Diffeomorphisms*, vol. 171. Springer, [3](#)
- [39] J. Duchon, "Interpolation des fonctions de deux variables suivant le principe de la flexion des plaques minces," *Revue Française d'Automatique, Informatique, Recherche Opérationnelle. Analyse Numérique*, vol. 10, no. R3, pp. 5–12, 1976. [3](#)
- [40] M. Nejati, R. Amirfattahi, and S. Sadri, "A fast hybrid approach for approximating a thin-plate spline surface," in *10th Iranian Conference on Electrical Engineering*, pp. 204–208, IEEE, 2010. [3](#)
- [41] F. L. Bookstein, "Principal warps: Thin-plate splines and the decomposition of deformations," *IEEE Transactions on Pattern Analysis and Machine Intelligence*, vol. 11, no. 6, pp. 567–585, 1989. [3](#)
- [42] B. S. Morse, T. S. Yoo, P. Rheingans, D. T. Chen, and K. R. Subramanian, "Interpolating implicit surfaces from scattered surface data using compactly supported radial basis functions," in *ACM SIGGRAPH*, pp. 78–es, 2005. [3](#)
- [43] S. P. Sastry, V. Zala, and R. M. Kirby, "Thin-plate-spline curvilinear meshing on a calculus-of-variations framework," *Procedia Engineering*, vol. 124, pp. 135–147, 2015. [3](#)
- [44] M. Jaderberg, K. Simonyan, A. Zisserman, and K. Kavukcuoglu, "Spatial transformer networks," in *Advances in Neural Information Processing Systems*, pp. 2017–2025, 2015. [3](#), [13](#), [14](#)
- [45] J. Li, Y. Chen, L. Cai, I. Davidson, and S. Ji, "Dense transformer networks," *arXiv preprint arXiv:1705.08881*, 2017. [3](#)
- [46] D. P. Kingma and J. Ba, "Adam: A method for stochastic optimization," *arXiv preprint arXiv:1412.6980*, 2014. [3](#), [7](#)
- [47] S. Lloyd, "Least squares quantization in pcm," *IEEE Transactions on Information Theory*, vol. 28, no. 2, pp. 129–137, 1982. [3](#)
- [48] E. Klassen, A. Srivastava, M. Mio, and S. H. Joshi, "Analysis of planar shapes using geodesic paths on shape spaces," *IEEE Transactions on Pattern Analysis and Machine Intelligence*, vol. 26, no. 3, pp. 372–383, 2004. [4](#)
- [49] A. Srivastava, S. H. Joshi, W. Mio, and X. Liu, "Statistical shape analysis: Clustering, learning, and testing," *IEEE Transactions on Pattern Analysis and Machine Intelligence*, vol. 27, no. 4, pp. 590–602, 2005. [4](#)
- [50] R. Balestrieri, "Symjax: symbolic cpu/gpu/tpu programming," *arXiv preprint arXiv:2005.10635*, 2020. [4](#)
- [51] Y. Yang, D. Xu, F. Nie, S. Yan, and Y. Zhuang, "Image clustering using local discriminant models and global integration," *IEEE Transactions on Image Processing*, vol. 19, no. 10, pp. 2761–2773, 2010. [4](#)
- [52] J. Xie, R. Girshick, and A. Farhadi, "Unsupervised deep embedding for clustering analysis," in *International Conference on Machine Learning*, pp. 478–487, 2016. [4](#), [8](#)
- [53] Z. Jiang, Y. Zheng, H. Tan, B. Tang, and H. Zhou, "Variational deep embedding: An unsupervised and generative approach to clustering," *arXiv preprint arXiv:1611.05148*, 2016. [4](#), [8](#)
- [54] D. Arthur and S. Vassilvitskii, "k-means++: The advantages of careful seeding," tech. rep., 2006. [7](#)
- [55] L. v. d. Maaten and G. Hinton, "Visualizing data using t-sne," *Journal of Machine Learning Research*, vol. 9, no. Nov, pp. 2579–2605, 2008. [8](#)
- [56] M. B. Wakin, D. L. Donoho, H. Choi, and R. G. Baraniuk, "The Multiscale Structure of Non-differentiable Image Manifolds," in *Wavelets XI*, vol. 5914, p. 59141B, International Society for Optics and Photonics, 2005. [13](#)

- [57] L. Deng, “The mnist database of handwritten digit images for machine learning research [best of the web],” *IEEE Signal Processing Magazine*, vol. 29, no. 6, pp. 141–142, 2012. 14
- [58] S. Becker, M. Ackermann, S. Lapuschkin, K.-R. Müller, and W. Samek, “Interpreting and explaining deep neural networks for classification of audio signals,” *arXiv preprint arXiv:1807.03418*, 2018. 14
- [59] R. Cosentino and B. Aazhang, “Learnable group transform for time-series,” in *International Conference on Machine Learning*, 2020. 15
- [60] G. Cohen, S. Afshar, J. Tapson, and A. Van Schaik, “Emnist: Extending mnist to handwritten letters,” in *International Joint Conference on Neural Networks*, pp. 2921–2926, IEEE, 2017. 15
- [61] L. Moroney, “Rock, paper, scissors dataset,” feb 2019. 15
- [62] N. Gourier, D. Hall, and L. J. Crowley, “Estimating face orientation from robust detection of salient facial structures,” *International Workshop on Visual Observation of Deictic Gestures*, 2004. 15
- [63] N. Altwaijry and I. Al-Turaiki, “Arabic handwriting recognition system using convolutional neural network,” *Neural Computing and Applications*, pp. 1–13, 2020. 15

7. Properties of DI K-means and Proofs

7.1. DI K-means Similarity Measure: a Quasipseudosemimetric

Proposition 2. *The similarity measure defined by $\min_{\nu \in \mathbb{R}^{2\ell}} \|TPS_\ell(x, \nu) - \mu\|$ is a Quasipseudosemimetric.*

Proof. Let's first define the orbit of an image with respect to the TPS transformations. Note that, the TPS does not form a group as it is a piecewise mapping. However, we know that it approximates the group of diffeomorphism on \mathbb{R}^2 . Therefore, for sake of simplicity, we will make a slight notation abuse by considering the orbit, equivariance, and others group specific properties as being induced by the TPS.

Definition 1. *We define the orbit an image x under the action the TPS_ℓ by*

$$\mathcal{O}(x) = \{TPS_\ell(x, \nu) | \nu \in \mathbb{R}^{2\ell}\}. \quad (6)$$

Let's now consider each metric statement:

- 1) It is non-negative as per the use of a norm.
- 2) **Pseudo:** $\min_{\nu \in \mathbb{R}^{2\ell}} \|(TPS_\ell(x, \nu) - \mu)\| = 0 \Leftrightarrow \exists \nu \in \mathbb{R}^{2\ell}, s.t. x = TPS_\ell(x, \nu) \Leftrightarrow x \sim_{TPS_\ell} \mu$, that is, x and μ are equivariant with respect to the transformations induced by TPS_ℓ . Thus, $d(x, \mu) = 0$ for possibly distinct values x and μ , however, these are not distinct when we consider the data as any possible point on their orbit with respect to the group of diffeomorphism. In fact, the distance is equal to 0 if and only if, μ and x are equivariant.
- 3) **Quasi:** The asymmetry of the distance is due to the non-volume preserving deformations considered. In fact, we do not consider the Haar measure of the associated diffeomorphism group and consider the L_2 distance with respect to the Lebesgue measure. Although the asymmetry of d does not affect our algorithm or results, a symmetric metric can be built by normalizing the distance by the determinant of the Jacobian of the transformation. Such a normalization would make the metric volume-preserving and as a result make the distance symmetric.
- 4) **Semi:** If $x, x', x'' \in \mathcal{O}$, then $d(x, x'') = d(x, x') = d(x', x'') = 0$ as it exist a ν, ν', ν'' such that the TPS maps each data onto the other as per definition of the orbit, thus the triangular inequality holds. If $x, x'' \in \mathcal{O}$ and $x' \notin \mathcal{O}$, we have $d(x, x'') = 0 \leq d(x, x') + d(x', x'')$. If $x, x' \in \mathcal{O}$ and $x'' \notin \mathcal{O}$, we have $d(x, x'') = d(x, x')$, and since $0 \leq d(x, x')$, the inequality is respected. However, if x, x', x'' belong to three different orbits, then we do not have the guarantee that then triangular inequality holds. In fact, it will depend on the distance between the orbits which is specific to each dataset. \square

7.2. DI K-means Updates: Proof of Proposition 1

We consider the F chet mean of the centroid k to be the solution of the following optimization problem, $\arg \min_{\mu_k} \sum_{i: x_i \in C_k} d(x_i, \mu_k)$. Using our similarity measure, we obtain the following.

Proof. The Fr chet mean for the cluster C_k is defined as $\arg \min_{\mu_k, \|\mu_k\|=1} \sum_{i: x_i \in C_k} \|TPS_\ell(x_i, \nu^*) - \mu_k\|^2$ since the optimization problem is convex in μ_k (as the result of the composition of the identity map and a norm which are both convex) we have $\mu_k^* : \nabla_{\mu} \sum_{i: x_i \in C_k} \|TPS_\ell(x_i, \nu^*) - \mu_k\|^2 + \lambda(\|\mu_k\| - 1) = 0$. with,

$$\nabla_{\mu} \sum_{i: x_i \in C_k} \|TPS_\ell(x_i, \nu^*) - \mu_k\|^2 + \lambda \|\mu_k\|^2 = 2(|C_k| + \lambda) \times \mu_k + 2 \sum_{i: x_i \in C_k} TPS_\ell(x_i, \nu^*). \quad (7)$$

\square

7.3. DI K-means Similarity Measure: Invariance Property

Motivated by the fact that small diffeomorphic transformations, usually, do not change nature of an image, we propose to exploit the invariance property of the similarity measure we proposed. We will also show that this invariance property induces generalization guarantees.

In this section, for sake of simplicity we will assume that the transformations belong to the group of diffeomorphism. In fact, the TPS can be considered as a method to sample element of this group.

Let's define an invariant similarity measure under the action of such group. That is, the similarity between two images remain the same under any diffeomorphic transformations. We propose to define the invariance in the framework of centroid-based clustering algorithm as follows.

Definition 2. An invariant similarity measure with respect to $\text{Diff}(\mathbb{R}^2)$ is defined as $d : \mathbb{R}^n \times \mathbb{R}^n \rightarrow \mathbb{R}^+$ such that for all images $x \in \mathbb{R}^n$, all centroids $\mu \in \mathbb{R}^2$, and all group elements $\forall g \in \text{Diff}(\mathbb{R}^2)$, we have

$$d(x, \mu) = d(g \star x, \mu), \quad (8)$$

where $g \star x$ denotes the action of the group element g onto the image x .

The similarity used in Eq. 3 of the optimization problem is $\text{Diff}(\mathbb{R}^2)$ -invariant as per Definition 2.

Proposition 3. The similarity $\min_{g \in \text{Diff}(\mathbb{R}^2)} \|g \star x - \mu\|$ is $\text{Diff}(\mathbb{R}^2)$ -invariant.

Proof. Let consider $g^* = \arg \min_{g \in \text{Diff}(\mathbb{R}^2)} \|g \star x - \mu\|$, we have $\arg \min_{g \in \text{Diff}(\mathbb{R}^2)} \|g \cdot g' \star x - \mu\| = g^* \cdot g'^{-1}$, where g'^{-1} is the inverse group element of g' . In fact, $\|g^* \cdot g'^{-1} \cdot g' \star x - \mu\| = \|g^* \star x - \mu\|$. Since for all $g' \in \text{Diff}(\mathbb{R}^2)$, it exists an inverse element g'^{-1} , we have that $\forall g \in \text{Diff}(\mathbb{R}^2)$, $d(g' \star x, \mu) = d(x, \mu)$.

That is, by definition of the group, there is always another element that minimizes the loss function by using the composition between the inverse element of the group that has just been added, g' , and the optimal element g^* . \square

8. Implementation Details

Note that the deformation invariant similarity measure we introduced in Eq. 3 differs from the affine invariant distances developed in [26, 34, 35]. All previously defined measures of error rely on the assumption that the manifold can be locally linearized and as a result the tangent space is used as a proxy to learn the optimal affine transformation. However, the work of [56] suggests that tangent planes fitted to image manifold continually twist off into new dimensions as the parameters of the affine transformations vary due to a possible the intrinsic multiscale structure of the manifold. As such, the alignment of two images can be done by linearizing the manifold. To do so, [56] propose to consider the multiscale structure of the manifold, we simplify their approach by applying a low-pass filter on the images and the centroid prior to learn the affine transformation best aligning them. Then, we optimize the remaining part of the TPS to account for diffeomorphic transformations. These two steps are similar to the one used in [44].

9. Neural Network Architectures

For both architectures, the decoder architecture is symmetric to the encoder and the batch size is set to 64.

MLP: The MLP architecture from input data to bottleneck hidden layer is composed of 4 fully connected ReLU layers with dimensions [500, 500, 2000, 10].

Conv: The CONV architecture is composed of 3 $2d$ -convolutional ReLU layers with 32 filters of size 5×5 , and 2 fully connected ReLU layers with dimension [400, 10]. For each layer, a batch normalization is applied.

10. Thin-Plate-Spline Interpolation

Let's consider two set of landmarks, the source ones $\nu_s = \{u_i, v_i\}_{i=1}^\ell$ and the transformed $\nu_t = \{u'_i, v'_i\}_{i=1}^\ell$ where ℓ denotes the number of landmarks. The TPS aim at finding a mapping $F = (F_1, F_2)$, such that $F(u, v) = (F_1(u, v), F_2(u, v)) = (u', v')$, that is, the mapping between two set of landmarks. The particularity of the TPS is that it learns such a mapping by minimizing the interpolation term, and a regularization that consists in penalizing the bending energy.

The TPS optimization problem is defined by

$$\min_F \sum_{i=1}^N \|(u'_i, v'_i) - F(u_i, v_i)\|^2 + \lambda \int \int \left[\left(\frac{\partial^2 F}{\partial u^2} \right)^2 + 2 \left(\frac{\partial^2 F}{\partial u \partial v} \right)^2 + \left(\frac{\partial^2 F}{\partial v^2} \right)^2 \right] dudv. \quad (9)$$

In our model, the source landmarks are consider to be the coordinates of a uniform grid. Also note that both the source landmarks and transformed ones are usually a subsets of the set of coordinate of the images. For instance, for the MNIST dataset of size 28×28 , the landmarks would be a grid of size $\ell \times \ell$, where $\ell < 28$. While the mapping is based on the landmark, it is then applied to the entire image coordinate. In fact, $F = (F_1, F_2)$ is mapping $\mathbb{R}^2 \rightarrow \mathbb{R}^2$, where F_1 (resp. F_2) corresponds to the mapping from (x, y) to the first dimension x' (resp. the second dimension y').

The solution of the TPS optimization problem, Eq. 9, provides the following analytical formula for F

$$F_1(u, v) = u' = a_1^{(1)} + a_u^{(1)}u + a_v^{(1)}v + \sum_{i=1}^{\ell} w_i^{(u)} U(|(u_i, v_i) - (u, v)|), \quad (10)$$

$$F_2(u, v) = v' = a_1^{(2)} + a_u^{(2)}u + a_v^{(2)}v + \sum_{i=1}^{\ell} w_i^{(v)} U(|(u_i, v_i) - (u, v)|), \quad (11)$$

where $|\cdot|$ is the L_1 -norm, a_1, a_u, a_v are the parameters governing the affine transformation, and w_i are parameters responsible for non-rigid transformations as they stand as a weight of the non-linear kernel U . The non-linear kernel U is expressed by $U(r) = r^2 \log(r^2), \forall r \in \mathbb{R}_+$.

Based on the landmarks ν_s and ν_t , we can obtain these parameters by solving a simple system of equation define by the following operations

$$\mathcal{L}^{-1}\mathcal{V} = \begin{bmatrix} (W^{(x)} | a_1^{(x)} a_x^{(x)} a_y^{(x)})^T \\ (W^{(x)} | a_1^{(y)} a_x^{(y)} a_y^{(y)})^T \end{bmatrix}. \quad (12)$$

where the matrix $\mathcal{L} \in \mathbb{R}^{(\ell+3) \times (\ell+3)}$, is defined as

$$\mathcal{L} = \left[\begin{array}{c|c} \mathcal{K} & \mathcal{P} \\ \hline \mathcal{P}^T & \mathcal{O} \end{array} \right], \mathcal{K} = \begin{bmatrix} 0 & U(r_{12}) & \dots & U(r_{1\ell}) \\ U(r_{21}) & 0 & \dots & U(r_{2\ell}) \\ \dots & \dots & \dots & \dots \\ U(r_{\ell 1}) & \dots & \dots & 0 \end{bmatrix}, \mathcal{P} = \begin{bmatrix} 1 & x_1 & y_1 \\ 1 & x_2 & y_2 \\ \dots & \dots & \dots \\ 1 & x_\ell & y_\ell \end{bmatrix}$$

where $r_{ij} = |(u_i, v_i) - (u_j, v_j)|$, $\mathcal{K} \in \mathbb{R}_+^{\ell \times \ell}$, and $\mathcal{V} = \begin{bmatrix} x'_1 & x'_2 & \dots & x'_\ell & 0 & 0 & 0 \\ y'_1 & y'_2 & \dots & y'_\ell & 0 & 0 & 0 \end{bmatrix}$.

Note that, since the matrix \mathcal{L} depends only on the source landmarks, and that in our case these are unchanged, its inverse can be computed only once. The only operation required to be computed for each data and each centroid is the matrix multiplication $\mathcal{L}^{-1}\mathcal{V}$ providing the parameters of the TPS transformation, as per Eq. 10, 11. Given these parameters, the mapping F can be applied to to each coordinate of the image.

Now in order to render the image, one can perform bilinear interpolation as it is achieved in . Besides, the bilinear interpolation will allow the propagation of the gradient through any differentiable loss function.

Given an image $x_1 \in \mathbb{R}^n$ where $n = W \times H$, W denotes the width and H the height of the image, and two sets of landmarks $\nu_s = \{u_i, v_i\}_{i=1}^{\ell}$, uniform grid coordinate of x_1 , and $\nu_t = \{u'_i, v'_i\}_{i=1}^{\ell}$, the transformation of the uniform grid, which are subset of the image coordinate, We are able to learn a mapping $F = (F_1, F_2)$ such that for each original pixel coordinate, we have their transformed coordinates. In fact, given any position (u, v) on the original image, the mapping F provides the new positions (u', v') as per Eq. 10, Eq. 11.

Now, from this transformed the coordinates space, we can render an image $x_2 \in \mathbb{R}^n$ using, as in [44], the bilinear interpolation function $\Gamma : \mathbb{R}^2 \times \mathbb{R}^n \rightarrow \mathbb{R}$ which takes as input the original image x_1 and the transformed pixel coordinates (u', v') , and outputs the pixel value of the transformed image at a given pixel coordinate

$$\begin{aligned} x_2(k, l) &= \Gamma[F(u_k, v_l), x_1] \\ &= \Gamma[(u'_k, v'_l), x_1] \\ &= \sum_{t, h \in \{0, 1\}} \sum_{i=1}^W \sum_{j=1}^H x_1(i, j) \delta(\lfloor u'_k + t \rfloor - i) \times \delta(\lfloor v'_l + h \rfloor - j) (u'_k - \lfloor u'_k \rfloor)^{\delta(t)} (v'_l - \lfloor v'_l \rfloor)^{\delta(h)} \\ &\quad \times (1 - (v'_l - \lfloor v'_l \rfloor))^{\delta(t-1)} (1 - (u'_k - \lfloor u'_k \rfloor))^{\delta(h-1)}, \end{aligned}$$

where δ is the Kronecker delta function and $\lfloor \cdot \rfloor$ is the floor function rounding the real coordinate to the closest pixel coordinate.

11. Datasets

MNIST [57]: is a handwritten digit dataset containing 60.000 training and 10.000 test images of dimension 28×28 representing 10 classes.

Aff. MNIST: we randomly sample one instance of each MNIST class and generate 100 random affine transformations for each sample. A third of the data are used for testing.

Diffeo. MNIST: we randomly sample one instance of each MNIST class and generate 100 random affine transformations for each sample as well as random diffeomorphisms using the TPS method. A third of the data are used for testing.

Audio MNIST [58]: is composed of 30000 recordings of spoken digits by 60 different speaker and sampled at $48kHz$ of 1sec long. It consists of 10 classes. We use 10000 data for testing and 20000 for testing. This dataset will be transformed into a time-frequency representation. This representations, can be considered as images, are usually used as the common

representation of audio recordings [59].

E-MNIST [60]: is a handwritten letters dataset merging a balanced set of the uppercase and lowercase letters into a single 26 classes dataset of dimension 28×28 .

Rock-Paper-Scissors [61]: images of hands playing rock, paper, scissor game, that is, a 3 classes dataset. The dimension of each image is 300×300 . The training set is composed of 2520 data and the testing set 372.

Face-10 [62]: images of the face of 15 people, wearing glasses or not and having various skin color. For each individual, different samples are obtained with different pose orientation varying from -90 degrees to $+90$ degrees vertical degrees. The dimension of each image is 288×384 . The training set is composed of 273 data and testing set of 117 data.

Arabic Char [63]: Handwritten Arabic characters written by 60 participants. The dataset is composed of 13, 440 images in the training set and 3360 in the test set. The dimension of each image is 32×32 .

12. Supplementary Visualisations

12.1. Additional t-SNE Visualisations

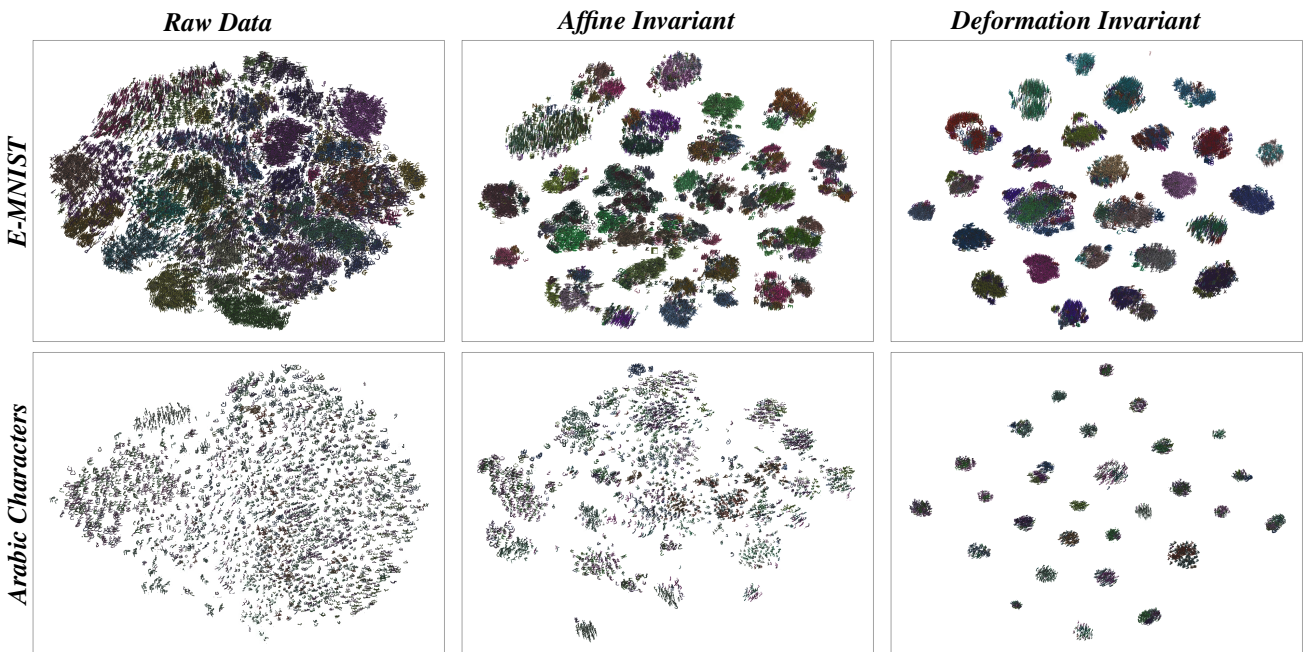


Figure 6: **2-dimensional t-SNE Visualisation** - The raw data (*left column*), the affinely transformed data, i.e., we extract the transformation of the data that corresponds to the centroid it was assigned and perform the t-SNE on these affinely transformed data, (*middle column*), the data transformed with respect to diffeomorphism as per Eq. 3, i.e., the same process as previously mentioned but we consider the transformation induced by the TPS, and then perform the dimension reduction on these transformed data, (*right column*). Each row corresponds to a different datasets, E-MNIST, Arabic Characters, are depicted from the top to bottom row. For all the figures, the colors of the data represent their ground truth labels.

12.2. Additional Centroid Visualisations

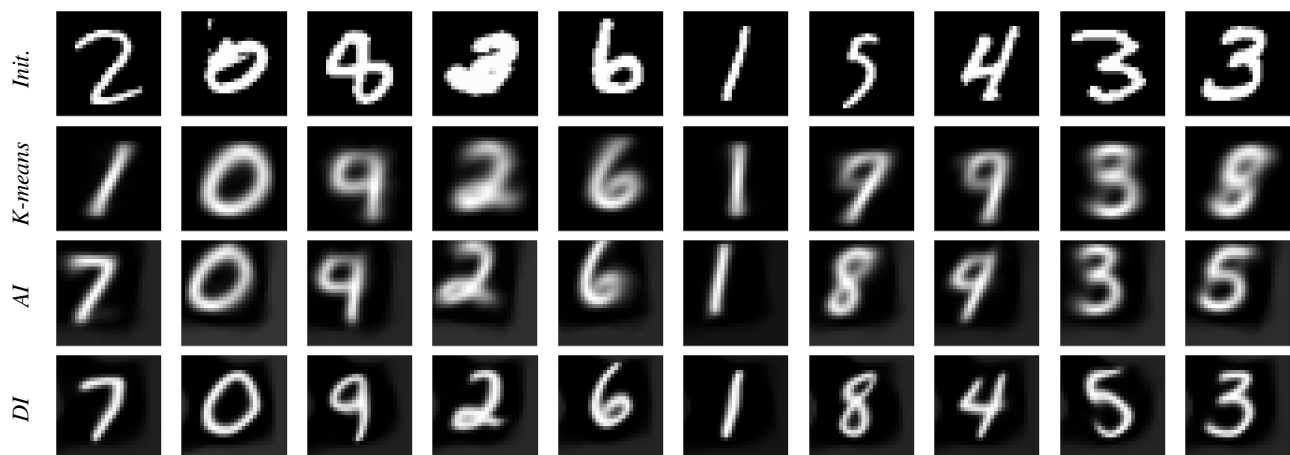


Figure 7: *Additional - MNIST Centroids Visualization (dim 28x28)* - Depiction of the initialization of the per-cluster centroids **top row** and the final per-cluster centroids of the K-means, Affine invariant K-means, and DI K-means (proposed) methods.

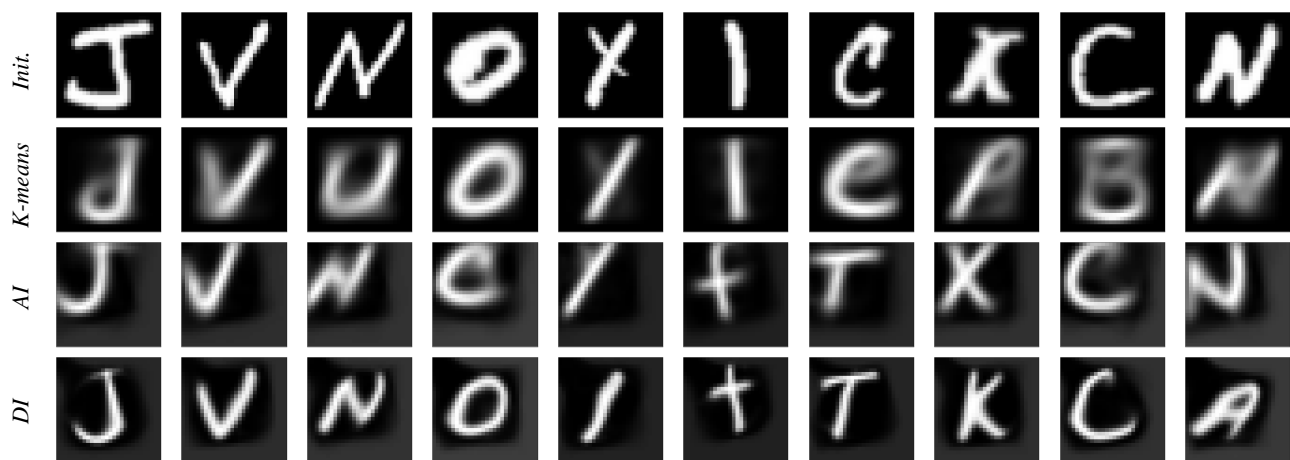


Figure 8: *Additional - 10 out of 26 EMNIST Centroids Visualization (dim 28x28)* - Depiction of the initialization of the per-cluster centroids **top row** and the final per-cluster centroids of the K-means, AI K-means, and DI K-means (proposed) methods.

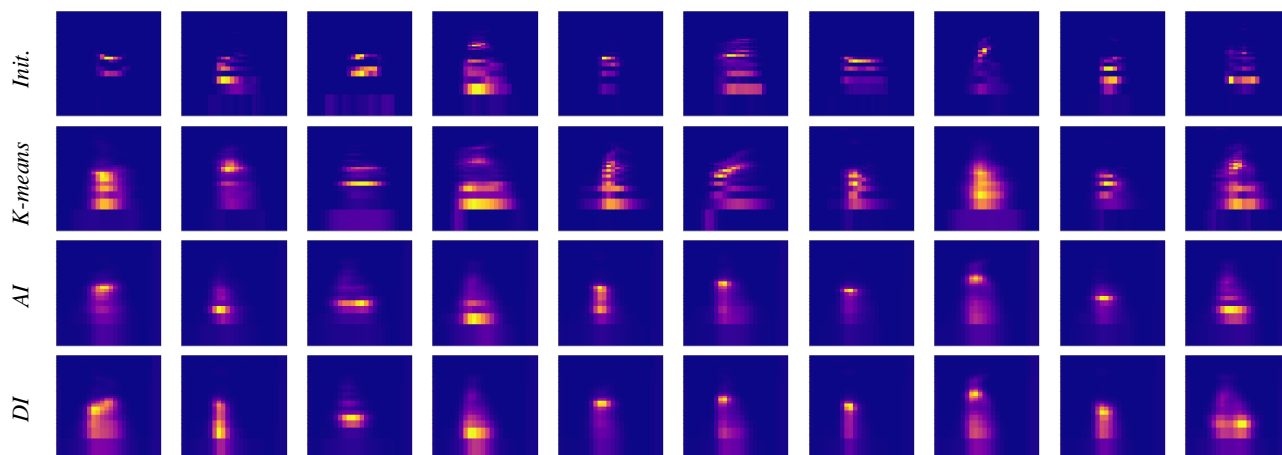


Figure 9: *Additional - Audio MNIST Centroids Visualization (dim 64x24)* - Depiction of the initialization of the per-cluster centroids **top row** and the final per-cluster centroids of the K-means, AI K-means, and DI K-means (proposed) methods.

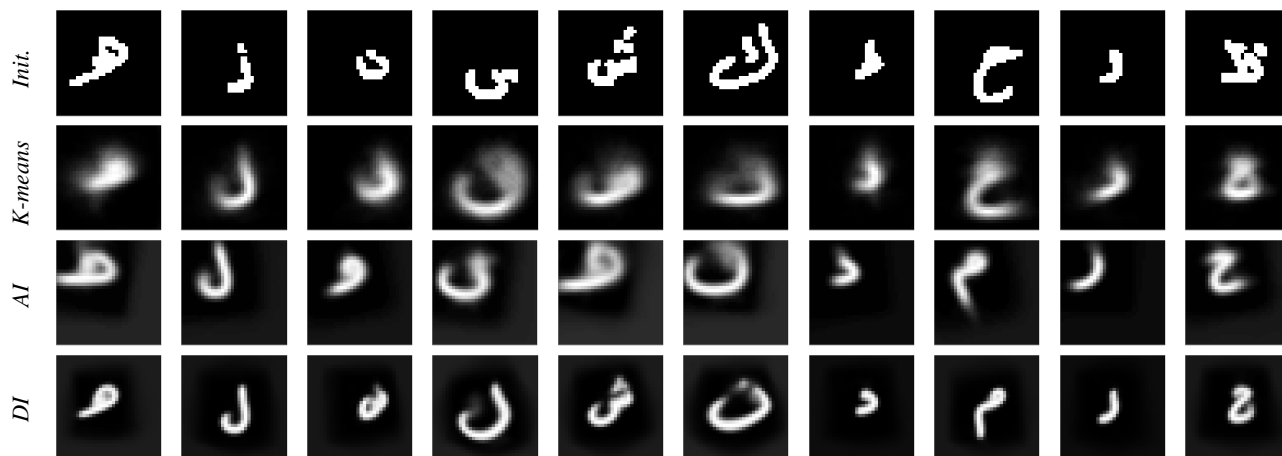


Figure 10: *Additional - 10 out of 28 Arab Characters Centroids Visualization (dim 32x32)* - Depiction of the initialization of the per-cluster centroids **top row** and the final per-cluster centroids of the K-means, AI K-means, and DI K-means (proposed) methods.



Figure 11: *Additional - 10 out of 13 Face Position Centroids Visualization (dim 288x384)* - Depiction of the initialization of the per-cluster centroids **top row** and the final per-cluster centroids of the K-means, AI K-means, and DI K-means (proposed) methods.